crystals

MDPI

Article

Investigation of the Effect of the Trifluoropropynyl Ligand on Pt(N^C^N)X (X = Cl, C_2CF_3) Complexes

John H. Zimmerman [1], Benjamin J. Cahill [1], Wilson M. Thomas [1], Jackson S. McCarthy [1], Colin D. McMillen [2,*] and Paul S. Wagenknecht [1,*]

[1] Department of Chemistry, Furman University, Greenville, SC 29613, USA
[2] Department of Chemistry, Clemson University, Clemson, SC 29634, USA
* Correspondence: cmcmill@clemson.edu (C.D.M.); paul.wagenknecht@furman.edu (P.S.W.)

Abstract: The tuning of the luminescent properties of Pt^{II} complexes for possible use in organic light-emitting diodes (OLEDs) and sensing applications is commonly achieved by altering the electronic properties of the ligands. Our group recently demonstrated that the trifluoropropynyl ligand is strongly electron-withdrawing and possibly useful for blueshifting emission. Herein, we report the synthesis of two complexes of this trifluoropropynyl ligand, namely $PtLC_2CF_3$ and $PtL^FC_2CF_3$ (L = 1,3-di(2-pyridyl)benzene; L^F = 4,6-difluoro-1,3-di(2-pyridyl)benzene). The $PtLC_2CF_3$ complex crystallized in the monoclinic space group $P2_1/n$ with Z = 4. The $PtL^FC_2CF_3$ complex crystalized in the triclinic space group *P*-1 with Z = 2. Changing the tridentate ligand from L to L^F resulted in a change in the packing structure, with the latter showing a metallophilic interaction (Pt-Pt distance = 3.3341(3) Å). The solution photophysics of the trifluoropropynyl complexes is compared with that of the corresponding Cl complexes, PtLCl and PtL^FCl. Replacement of the chloro ligand with the trifluoropropynyl ligand blueshifted the monomer emission by less than 5 nm but blueshifted the excimer emission peaks by 15–20 nm. The complexes of the trifluoropropynyl ligand also favor the excimer emission more than the complexes of the chloro ligand. The excimer emission is quenched by dissolved oxygen significantly more than the corresponding monomer emission. The excimer emission and monomer emission are well separated, and the ratio of monomer to excimer emission is strongly dependent on oxygen concentration.

Keywords: phosphorescence; OLED; platinum(II); excimer; oxygen sensor

Citation: Zimmerman, J.H.; Cahill, B.J.; Thomas, W.M.; McCarthy, J.S.; McMillen, C.D.; Wagenknecht, P.S. Investigation of the Effect of the Trifluoropropynyl Ligand on Pt(N^C^N)X (X = Cl, C_2CF_3) Complexes. *Crystals* **2024**, *14*, 678. https://doi.org/10.3390/cryst14080678

Academic Editor: Vladimir P. Fedin

Received: 8 July 2024
Revised: 19 July 2024
Accepted: 21 July 2024
Published: 25 July 2024

1. Introduction

Recently, there has been substantial research into improving the performance of organic light-emitting diodes (OLEDs) for use in digital displays and lighting applications. A variety of organometallic Ir^{III}- and Pt^{II}-luminophores have been studied for use in OLEDs because the high spin–orbit coupling (SOC) constants associated with these metals [1] enable the harvesting of both singlet and triplet excitons [2]. In particular, these organometallic luminophores are actively researched for use in the manufacture of efficient deep-blue OLEDs, which has proven to be challenging [3,4]. Additionally, deep-blue emitters are desirable for white OLED (WOLED) applications, as deep-blue light can be mixed with orange light and appear white to a human observer [5,6].

The ground electronic state of Pt^{II} complexes is a singlet ground state (^{1}GS), i.e., all electrons are paired. Spin-allowed excitation results in a singlet excited state (^{1}ES) which can undergo intersystem crossing (ISC) to a triplet excited state (^{3}ES) (Figure 1). To produce deep-blue-emitting Pt^{II} luminophores, it is necessary to increase the energy gap between the ^{1}GS and the emissive ^{3}ES, which often has some triplet metal-to-ligand charge-transfer (^{3}MLCT) character [7–12]. Thus, it is helpful to utilize electron-withdrawing ligands to stabilize the HOMO. However, it is sometimes the case that increasing the energy of the emissive ^{3}ES causes the metal-centered ^{3}d-d state to become thermally accessible through

internal conversion (IC), which diminishes the efficiency of emission because the ^{3}d-d state undergoes rapid nonradiative (nr) decay (Figure 1) [4,13–15]. Therefore, it is beneficial to utilize ligands that are both high-field and electron-withdrawing to maintain the energy gap between the emissive ^{3}ES and the ^{3}d-d state, while increasing the energy of emission.

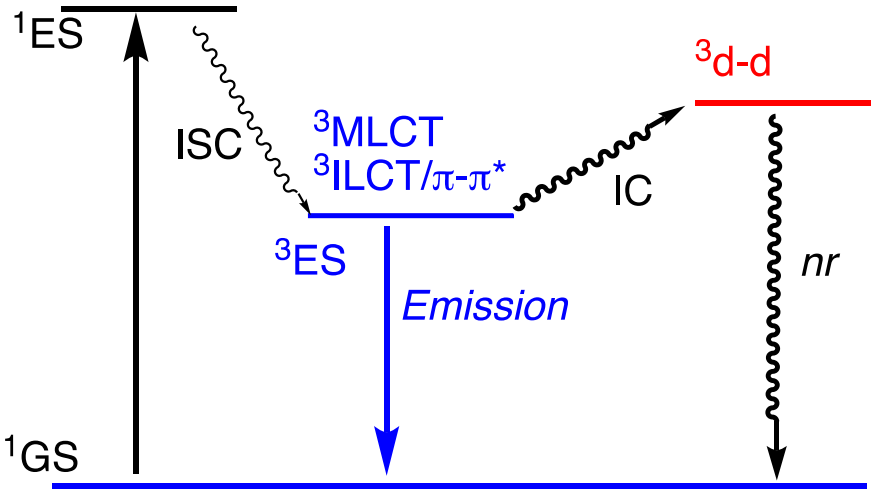

Figure 1. Modified Jablonski diagram showing initial spin-allowed excitation from a singlet ground state (^{1}GS) to a singlet excited state (^{1}ES). Intersystem crossing (ISC) results in an emissive triplet excited state (^{3}ES), which is often of mixed character involving triplet metal-to-ligand charge transfer (^{3}MLCT) character, triplet intraligand charge transfer (^{3}ILCT) character, and localized triplet π-π* character. Thermal access of the ^{3}d-d state through internal conversion (IC) results in rapid nonradiative (nr) decay, lowering the efficiency of emission.

Our group reported that the trifluoropropynyl ligand (:C≡C–CF_3) is more electron-withdrawing and higher field than the pentafluorophenylethynyl ligand (:C≡C–C_6F_5) [16], a ligand commonly used for its electron-withdrawing behavior. Recently, we showed that for Pt^{II} complexes with bidentate bipyridine ligands, utilizing the trifluoropropynyl ligand instead of the pentafluorophenylethynyl ligand blueshifted the emission and raised the ^{3}MLCT energy beyond that of the ^{3}π-π*, leading to a change in emissive ^{3}ES character [7]. Therefore, it may be advantageous to synthesize Pt^{II} luminophores with the trifluoropropynyl ligand to achieve efficient deep-blue emission.

The cyano-ligand has also been used to blueshift emission and maintain emission efficiency. The Shinozaki group showed that replacement of the Cl ligand with the CN ligand contributed to a blueshift in emission for Pt(Fmdpb)CN (FmdpbH=4-fluoro-1,3-di(4-methyl-2-pyridyl)benzene; Figure 2) and reported that additionally Pt(Fmdpb)CN emits more efficiently when compared to Pt(Fmdpb)Cl [17]. Because the :C≡C–CF_3 ligand has been shown to have similar electronic properties to the CN ligand [18], replacing the chloro ligand of NˆCˆN-chelated Pt^{II} complexes with the trifluoropropynyl ligand may indeed lead to more efficient and bluer emission. Thus, $PtLC_2CF_3$ and $PtL^FC_2CF_3$ (Figure 2; L = 1,3-di(2-pyridyl)benzene; L^F = 4,6-difluoro-1,3-di(2-pyridyl)benzene) were synthesized. Pt^{II} complexes with L and L^F ligands were chosen for this study as PtLCl and PtL^FCl have been investigated extensively by the Shinozaki group [17,19] and the Williams group [11,13,20,21] and emit blue-green (491 nm) and turquoise (472 nm) light, respectively.

Herein, we present the synthesis and characterization of $PtLC_2CF_3$ and $PtL^FC_2CF_3$. Solution-phase absorption and emission spectra as well as the related photophysical constants are reported. Excited-state aggregation into excimers (a common phenomenon among square planar Pt^{II} complexes) [7,20,22,23] is observed, and the excimer formation is explored. Additionally, the photophysical effects of rigidification in poly (methyl methacrylate) (PMMA) films are discussed, and the practicality of utilizing $PtLC_2CF_3$ and $PtL^FC_2CF_3$ in OLED applications is addressed.

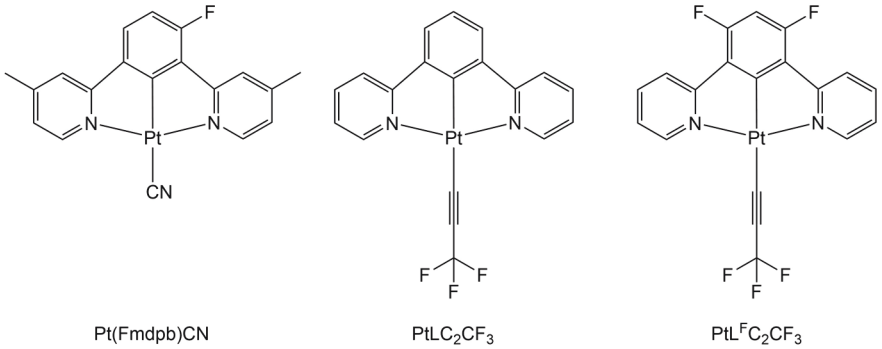

Pt(Fmdpb)CN $PtLC_2CF_3$ $PtL^FC_2CF_3$

Figure 2. Pt(Fmdpb)CN reported by the Shinozaki group [16] and the $PtLC_2CF_3$ and $PtL^FC_2CF_3$ investigated herein. The general designation for these terdentate ligands is N^C^N.

In addition, in the course of these investigations, we found that for PtLCl, $PtLC_2CF_3$, PtL^FCl, and $PtL^FC_2CF_3$ the well-separated excimer emission and monomer emission each exhibit different sensitivities to oxygen concentration in the form of oxygen quenching. Thus, it is possible to establish a ratiometric relationship between the oxygen concentration and the ratio of excimer/monomer emission intensity. Differential sensitivities of monomer and excimer to oxygen for $Pt(dtbpy)(CN)_2$ (dtbpy = 4,4′-di-*tert*-butyl-2,2′-bipyridine) and $Pt(bathophen)(CN)_2$ (bathophen = 4,7-diphenyl-l,10-phenanthroline) have previously been noted and these complexes suggested as oxygen-sensing materials [24]. Thus, the ratiometric response of the excimer/monomer emission ratio of PtLCl, $PtLC_2CF_3$, PtL^FCl, and $PtL^FC_2CF_3$ was probed and is discussed herein.

2. Materials and Methods

2.1. General Methods

UV–Vis: Absorption spectra were collected using a Cary-50 UV–vis spectrophotometer (Agilent Technologies, Santa Clara, CA, USA).

Emission Spectra: Emission spectra were collected using a Horiba Scientific (Piscataway, NJ, USA) Fluorolog-3 spectrofluorometer equipped with a FL-1013 liquid nitrogen dewar assembly for 77 K measurements and a J-1933 solid-sample holder for film measurements. All emission spectra were corrected for the response factor of the R928 photomultiplier tube using the factory correction files. Emission spectra involving excimer emission were additionally corrected with blank subtraction.

Excitation spectra: Excitation spectra were collected using a Horiba Scientific Fluorolog-3 sprectrofluorometer.

Emission Lifetime: Emission lifetimes were measured using a Photon Technology International (PTI, Lawrenceville, NJ, USA) GL-3300 pulsed nitrogen laser fed into a PTI GL-302 dye laser as the excitation source. The resulting data set was collected on an OLIS (Athens, GA, USA) SM-45 EM fluorescence lifetime measurement system using a Hamamatsu (Bridgewater, NJ, USA) R928 photomultiplier tube fed through a variable feed-through terminator into a LeCroy (Chestnut Ridge, NY, USA) WaveJet 352A oscilloscope and analyzed using OLIS Spectral Works.

NMR spectra: ^{1}H NMR spectra were obtained using a JEOL (Peabody, MA, USA) JNM-ECZR (500 MHz) spectrometer.

Elemental analysis: Elemental analyses were performed by Midwest Microlabs (Indianapolis, IN, USA).

Quantum Yields of Photoluminescence (Φ_{PL}): Relative solution-state photoluminescence quantum yields (Φ_{PL}) in CH_2Cl_2 were determined using solutions that were absorbance-matched with solutions of quinine sulfate (Φ_{PL} = 0.546) in 0.1 M H_2SO_4.

Thin Films: PMMA films for spectroscopy were prepared by dissolving PMMA (123 mg, M_w ~ 120,000) and the appropriate complex in CH_2Cl_2 (1 mL) solution. The mass of the complex was chosen to achieve the desired complex/PMMA mass percent. The solution was pipetted onto a quartz slide that was set at a 45° angle in a vial. The vials

were covered with a Kimwipe and the film allowed to cure overnight. These film-coated quartz slides were mounted in the solid-sample holder for emission measurements with the film facing the excitation source at a 112.5° angle.

Monomer/Excimer Emission Ratio Under Different [O_2] Concentrations: A solution of the desired platinum complex (≈1 × 10^{-4} M) was prepared in CH_2Cl_2 in a cuvette with a septum top without exclusion of air, and the emission spectrum was recorded. The sample was then sparged with O_2 for 10 min and the emission spectrum was recorded. The sample was then sparged with Ar for 10 min and the emission spectrum was recorded. The sparge gases were presaturated by bubbling through CH_2Cl_2 in order to minimize solvent evaporation.

2.2. Synthesis

PtLCl [25] and PtL^FCl [26] were prepared according to the literature procedures, with the exception that PtL^FCl was sufficiently pure, without the need for recrystallization. 1,3-di(2-pyridyl)benzene for the synthesis of PtLCl was purchased from AmBeed (Arlington Heights, IL, USA). 4,6-difluoro-1,3-di(2-pyridyl)benzene for the synthesis of PtL^FCl was prepared by a modification of the literature procedure [25]. In particular, the purification following the synthesis of the L^F ligand using a Stille coupling did not require column chromatography; rather, the initial solid was simply washed with a 3:1 hexanes/ether mixture, resulting in product that was sufficiently pure for coordination of the Pt. 3,3,3-trifluoro-1-propyne was obtained from Synquest Laboratories (Alachua, FL, USA). Sodium methoxide (25 wt % in methanol) was obtained from Sigma Aldrich (St. Louis, MO, USA). Poly(methyl methacrylate) was obtained from Sigma-Aldrich. All reactions were performed in oven-dried glassware under an argon atmosphere using an argon manifold.

General Synthetic Method: An oven-dried two-necked round-bottom flask under a positive pressure of Ar was charged with sodium methoxide (25% in CH_3OH) and degassed CH_3OH/CH_2Cl_2 (3:1 *v*:*v*). The valve to the Ar manifold was then closed and a positive pressure of Ar was maintained using an Ar-filled balloon attached to the flask through a short cannula. While the solution was stirring, 3,3,3-trifluoropropyne gas was slowly injected (2 min) into the solution through a septum and allowed to react for 2 h. A separate single-necked round-bottom flask under Ar was charged with the appropriate Pt precursor in degassed CH_3OH/CH_2Cl_2 (3:1 *v*:*v*). This Pt precursor solution/suspension was injected into the trifluoropropyne solution, and the resulting mixture was stirred for 24 h. The solvent was removed under reduced pressure and the remaining solid was purified using column chromatography (silica gel, 2.5 cm × 15 cm), eluting with 4:1 dichloromethane/hexanes. Due to the emissive nature of the product, the column was monitored with long-wavelength UV irradiation. The first band was collected, and the solvent was removed under reduced pressure. The resulting solid was suspended in diethylether and the product was collected using vacuum filtration.

PtLC_2CF_3: The general procedure was followed using PtLCl (0.1027 g, 0.222 mmol, 1 eq) in 5 mL of solvent, and 3,3,3-trifluoropropyne(g) (15 mL, 0.61 mmol, 3.5 eq) and NaOMe (0.10 mL, 0.46 mmol, 2.7 eq) in 12 mL of solvent, yielding 0.0898 g (77%). Anal. Calc (found) for $PtC_{19}H_{11}N_2F_3$: H, 2.13 (2.09); C, 43.94 (43.64); N, 5.39 (5.39)%. ^{1}H NMR (500 MHz, DMSO-d_6). δ 8.96 (m, 2H), 8.22 (m, 2H), 8.11 (m, 2H), 7.79 (d 2H), 7.52 (m, 2H), 7.27 (t, 1H). UV–Vis (CH_2Cl_2): λ_{max}/nm (ε/Lmol^{-1}cm^{-1}) 337 (7930), 367 (7890), 381 (9820). Rf 4:1 dichloromethane/hexanes = 0.5.

Pt$L^FC_2CF_3$: The general procedure was followed using PtL^FCl (0.1996 g, 0.40 mmol, 1 eq) in 20 mL of solvent, and 3,3,3-trifluoropropyne(g) (40 mL, 1.63 mmol, 4 eq) and NaOMe (0.40 mL, 1.85 mmol, 4.6 eq) in 24 mL of solvent, yielding 0.0824 g (37%). Anal. Calc (found) for $PtC_{19}H_9N_2F_5$: H, 1.63 (1.84); C, 41.09 (41.55); N, 5.04 (5.17)%. ^{1}H NMR (500 MHz, $CDCl_3$) δ 9.19 (m, 2H), 7.97 (m, 2H), 7.91 (d, 2H), 7.26 (m, 2H) (obscured), 6.64 (t, 1H). UV–vis (CH_2Cl_2) λmax/nm (ε/L mol^{-1} cm^{-1}) 323 (9540), 337 (13,500), 359 (8230). Rf 4:1 dichloromethane/hexanes = 0.6.

2.3. Single-Crystal X-ray Diffraction

Single-crystal X-ray diffraction data were collected at 100 K using a Bruker (Madison, WI, USA) D8 Venture diffractometer. The data were collected using phi and omega scans (0.5° oscillations) with a Cu Kα (λ = 1.54178 Å) microfocus source and a Photon 2 detector. Data were processed (SAINT) and corrected for absorption (multi-scan, SADABS), using the Apex3 suite [27]. The structures were solved by intrinsic phasing (SHELXT) and subsequently refined by full-matrix least squares on F^2 (SHELXL) [28,29]. All non-hydrogen atoms were refined anisotropically. Hydrogen atoms attached to carbon atoms were refined in calculated positions using riding models where $U_{eq}(H) = 1.2U_{eq}(C)$. Crystallographic data are summarized in Table 1. CCDC 2364563-2364564 contain the complete supplementary crystallographic data for this paper and can be obtained from the Cambridge Crystallographic Data Centre.

Table 1. Crystallographic data and refinement details for $PtLC_2CF_3$ and $PtL^FC_2CF_3$.

	$PtLC_2CF_3$	**$PtL^FC_2CF_3$**
Empirical Formula	$C_{19}H_{11}F_3N_2Pt$	$C_{19}H_9F_5N_2Pt$
F. W. (g/mol)	519.39	555.37
Temperature (K)	100(2)	100(2)
Crystal System	Monoclinic	Triclinic
Space group	$P2_1/n$	P-1
a (Å)	11.7293(5)	8.0971(7)
b (Å)	7.8617(4)	8.9919(7)
c (Å)	18.1664(8)	11.5368(9)
α (°)	90	98.714(2)
β (°)	107.5583(14)	103.405(2)
γ (°)	90	100.939(2)
Volume (Å^3)	1597.12(13)	785.26(11)
Z	4	2
D(calcd) (g/cm^3)	2.160	2.349
Wavelength (Å)	1.54178	1.54178
μ, mm^{-1}	16.769	17.306
F(000)	976	520
Crystal Size (mm)	0.05 × 0.23 × 0.26	0.04 × 0.11 × 0.12
θ range (°)	5.316 to 72.243	5.777 to 70.259
Reflections collected	32,402	26,668
Independent reflections	3158	2969
R(int)	0.0526	0.0370
No. of parameters	226	244
No. of restraints	0	0
R indices (I > 2σ(I))	R_1 = 0.0283 [a] wR_2 = 0.0855 [b]	R_1 = 0.0168 [a] wR_2 = 0.0425 [b]
R indices (all data)	R_1 = 0.0288 [a] wR_2 = 0.0863 [b]	R_1 = 0.0168 [a] wR_2 = 0.0425 [b]
Goodness-of-fit on F^2	1.118	1.157
Largest diff. peak/hole (e/Å^3)	2.864, −1.175	1.549, −0.685

[a] $R_1 = \Sigma||F_o| - [F_c||/\Sigma|F_o|$. [b] $wR_2 = \{\Sigma[w(F_o^2 - F_c^2)^2]/\Sigma[wF_o^2]^2\}^{1/2}$.

2.4. Computational Methods

Gaussian 16 [30] was used for all DFT and TDDFT calculations. Computational models involved the functional B3LYP [31] and the basis sets 6-31G(d) [32] and LANL2DZ [33]. GaussView version 6 [34] was used for all orbital imaging. GaussSum3 [35] was used for Mulliken population analysis.

3. Results and Discussion

3.1. Syntheses and Structural Characterization

The precursor complexes, PtLCl [25] and PtL^FCl [26], were prepared using slight modifications of the literature procedures. Ligand substitution of an alkynyl ligand for chloride on Pt^{II} complexes typically follows a CuI-catalyzed procedure derived from Sonogashira et al. [8,36,37]. For these complexes, however, we found this method to result in a product mixture that was not easily purified. Several reports of substituting alkynyl ligands for Cl on Pt(N^C^N) complexes have used an alternate procedure that did not use a catalyst, but instead used a strong base such as NaOMe or NaOH (Figure 3) [11,38,39]. This procedure gave the desired products that were easily purified by column chromatography. Only one equivalent of the alkynyl anion is necessary for the reaction but an excess (2–5 eq) was used in all attempted syntheses. The equivalents of the alkynyl anion that can form can be controlled by both the amount of NaOMe and trifluoropropyne added, and it is not necessary that all of the alkyne be deprotonated. The reaction did not appear to be significantly impacted by whether NaOMe or trifluoropropyne was in excess. Though the syntheses are performed under air-free conditions, the final products are air- and moisture-stable and can be handled as solids and in solution under ambient atmosphere.

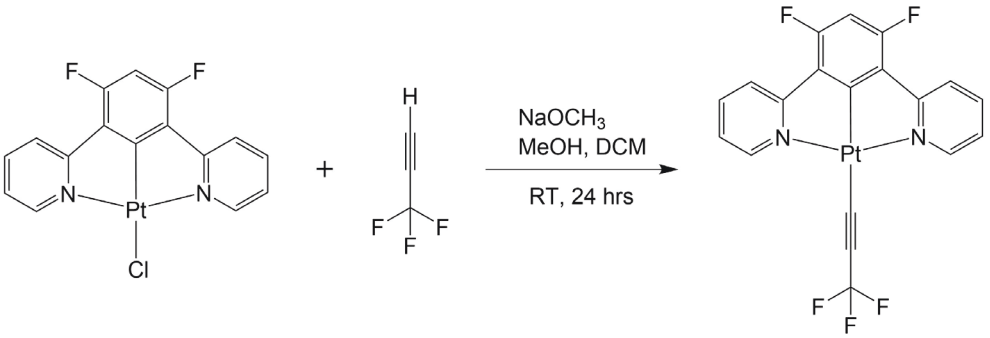

Figure 3. Synthesis of Pt$L^F C_2CF_3$. The synthesis of PtLC_2CF_3 follows the same procedure.

Crystals of PtLC_2CF_3 and Pt$L^F C_2CF_3$ were grown from the diffusion of diethyl ether into a CH_2Cl_2 solution of the complex, and slow evaporation of THF, respectively. For both complexes, the Pt is in a distorted square planar coordination environment (Figure 4, Tables 1 and 2), with similar angles enforced by the L and L^F ligands. The C–Pt–C angles show some deviation between the complexes (179.52(17)° for PtLC_2CF_3 versus 174.86(11)° for Pt$L^F C_2CF_3$). This deviation from linearity for Pt$L^F C_2CF_3$ continues along the alkynyl bond angles, with Pt–C≡C and C≡C-CF_3 bond angles of 172.3(3)° and 170.6(3)°, respectively (compared to 177.1(4)° and 177.0(5)° in PtLC_2CF_3). In this way, the :C≡C–CF_3 ligand is noticeably bent in Pt$L^F C_2CF_3$. The C≡C (C1-C2) bond lengths for both PtLC_2CF_3 (1.221 Å) and Pt$L^F C_2CF_3$ (1.208 Å) are in the normal range for alkynes, giving no indication that the distortion from linearity for Pt$L^F C_2CF_3$ is due to a reduction in the C≡C bond order. Thus, weak packing forces are likely the cause for these deviations from linearity. Indeed, the CF_3 groups of Pt$L^F C_2CF_3$ participate in three C–H···F short contacts with favorable distances and geometries enabled by the bent nature of the :C≡C–CF_3 ligand (Supplementary Materials, Figure S4). In PtLC_2CF_3, only one C–H···F contact is made (Supplementary Materials, Figure S3), as the packing of neighboring molecules restricts favorable C–H···F angles so that a bent :C≡C–CF_3 ligand is not imposed. Deviations from nonlinearity for RHgC_2CF_3 complexes have also been observed and attributed to intermolecular interactions within the crystal [40].

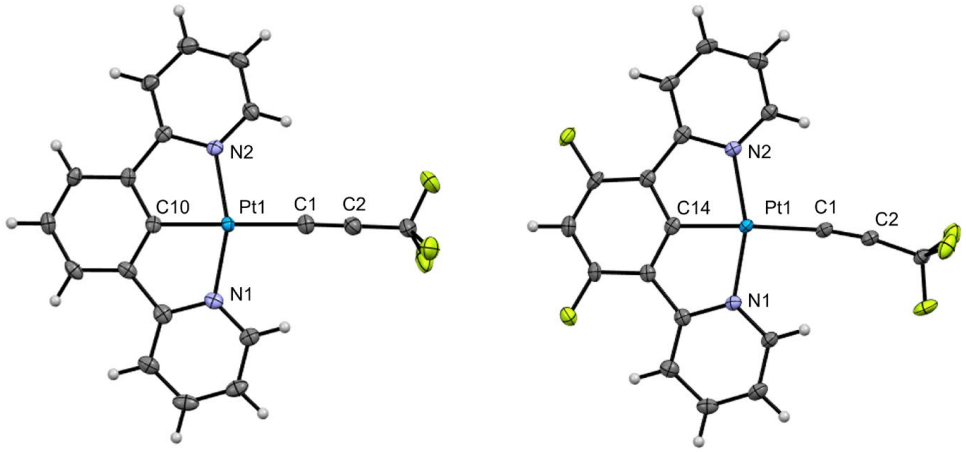

Figure 4. Structures of the $PtLC_2CF_3$ (**left**) and $PtL^FC_2CF_3$ (**right**) complexes with displacement ellipsoids shown at 50% probability levels. Platinum atoms are blue, fluorine atoms are lime green, nitrogen atoms are purple, carbon atoms are gray, and hydrogen atoms are white.

Table 2. Selected interatomic distances (Å) and plane-to-plane distances (Å) for Pt complexes.

	Pt-C_{NCN}	**Pt-N1**	**Pt-N2**	**Pt-X**	**Pt···Pt**	**Pt···Plane**
PtLCl [a]	1.907(8)	2.033(6)	2.041(6)	2.417(2)	4.85	3.40
$PtLC_2CF_3$	1.942(4)	2.040(3)	2.034(3)	2.034(4)	5.18	3.27
PtL^FCl [b]	1.910(6)	2.028(5)	2.043(5)	2.4124(15)	3.42	3.38
$PtL^FC_2CF_3$	1.939(3)	2.036(2)	2.037(2)	2.042(3)	3.34	3.33

[a] From [25], X-ray crystallography performed at 296 K. [b] From [26], X-ray crystallography performed at 298 K.

In $PtLC_2CF_3$, the complexes have a classic herringbone packing arrangement. Stacks of offset complexes have plane–plane separations of 3.27 Å, suggesting moderate pi···pi interactions (Figure 5). Neighboring stacks interact through C–H···pi interactions (Supplementary Materials, Figure S3). Because of the offset within a given stack, the Pt atoms do not line up right over one another, so there is no short Pt···Pt contact. For $PtL^FC_2CF_3$, on the other hand, neighboring complexes stack along the *a*-axis (Figure 5). This occurs through alternating Pt···Pt and offset pi stacking interactions with plane-to-plane separations of 3.33 Å, with neighboring stacks connected through C–H···F interactions (Supplementary Materials, Figure S4). The resulting Pt···Pt distance (3.3441(3) Å) is less than the sum of van der Waals radii (3.50 Å) [41], indicating a metallophilic interaction between Pt centers (Figure 6) [42,43]. This presence of solid-state Pt···Pt interactions for $PtL^FC_2CF_3$ likely contributes to the color of the crystals being red/orange, whereas crystals of the corresponding $PtLC_2CF_3$ complex are yellow. This is due to lower-energy absorptions to the singlet metal–metal-to-ligand charge transfer (^{1}MMLCT) state that are not present in the absence of such Pt···Pt interactions [44].

A structural comparison with the corresponding chloro analogues (Table 2) demonstrates that replacement of Cl with C_2CF_3 increases the Pt–C_{NCN} bond distance (Pt-C10 for $PtLC_2CF_3$ and Pt-C14 for $PtL^FC_2CF_3$) by approximately 0.03 Å for both analogues, likely an indication of the stronger trans influence of the :C≡C–CF_3 ligand. Furthermore, the presence of Pt···Pt contacts less than the sum of van der Waals radii appears to be more dependent on the identity of the NˆCˆN ligand than the X ligand (X = Cl, C_2CF_3), as such contacts are only present for the L^F complexes.

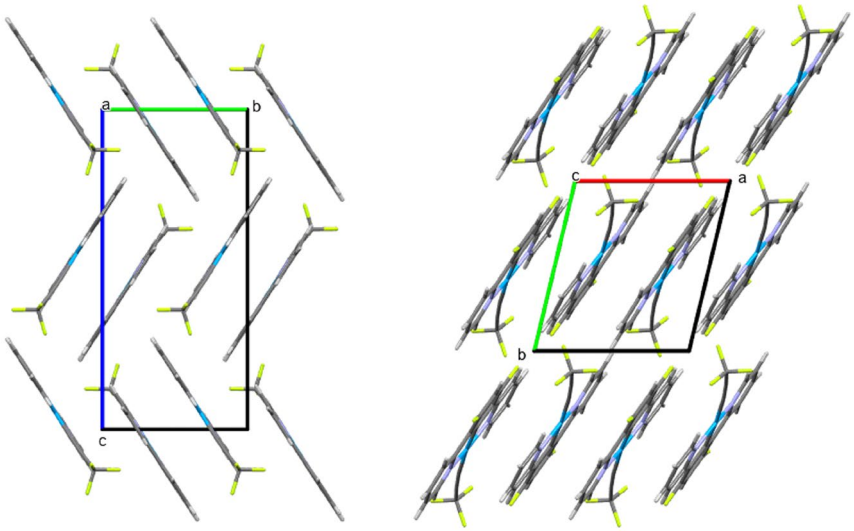

Figure 5. Packing of complexes in the structures of $PtLC_2CF_3$ (**left**, viewed along the *a*-axis) and $PtL^FC_2CF_3$ (**right**, viewed along the *c*-axis). Platinum atoms are blue, fluorine atoms are lime green, nitrogen atoms are purple, carbon atoms are gray, and hydrogen atoms are white.

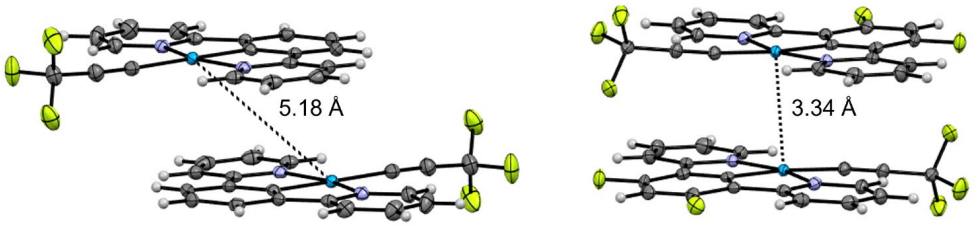

Figure 6. Shortest Pt···Pt distances in the stacked complexes of $PtLC_2CF_3$ (**left**) and $PtL^FC_2CF_3$ (**right**). Platinum atoms are blue, fluorine atoms are lime green, nitrogen atoms are purple, carbon atoms are gray, and hydrogen atoms are white.

3.2. Photophysical Characterization

3.2.1. Absorption Spectra

The absorption spectra of $PtLC_2CF_3$ and $PtL^FC_2CF_3$ are similar in shape to their chloro analogues, with a slight blueshift of the onset of the lowest-energy absorptions (Figure 7, Supplementary Materials, Table S3). These lowest-energy absorptions have been ascribed to excitation to an excited state of mixed orbital parentage, namely one with ^{1}MLCT/^{1}IL(π-π^*) character for many Pt^{II} complexes [8,11,22,37,45] including the chloro analogues [9,21]. This latter component can involve both localized $^1\pi$-π^* and ^{1}ILCT transfer from the phenyl to the pyridine. By analogy, the peaks in this range for $PtLC_2CF_3$ and $PtL^FC_2CF_3$ have been assigned as representing excitation into a mixed ^{1}MLCT/^{1}ILCT (π-π^*) excited state. In addition, both complexes show sharp weak absorptions on the red tail of these CT absorptions (Supplementary Materials, Figure S7). These have been previously observed for the chloro analogues and have been assigned to spin-forbidden excitation into the ^{3}ES [20,21]. Lastly, plots of absorbance vs. concentration (measured up to ~1×10^{-4} M) are linear (Supplementary Materials, Figure S8), indicating a lack of ground-state aggregation.

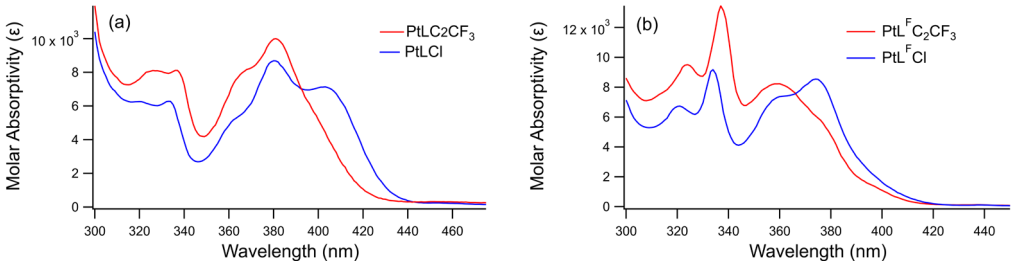

Figure 7. Overlay of the absorbance spectra of (**a**) PtLX complexes and (**b**) PtL^FX complexes in RT CH_2Cl_2 solution.

3.2.2. Monomer Emission Spectra

The emission spectra of $PtLC_2CF_3$ and $PtL^FC_2CF_3$ in a room-temperature (RT) CH_2Cl_2 solution (≈2.0×10^{-6} M) have well-defined peaks between 450 and 600 nm, with a clear vibronic progression (Figure 8, Supplementary Materials, Table S4). For each complex, the excitation spectrum agrees well with the absorbance spectrum (Supplementary Materials, Figure S9) indicating that the recorded emission is not due to an impurity. The vibronic progressions in the emission spectra are between 1230 and 1300 cm^{-1}. Such progressions have been attributed to emission from a ^{3}ILCT state in related complexes [37,45–47]. The replacement of the chloro ligand with the trifluoropropynyl ligand resulted in less than a 5 nm blueshift for both complexes. Thus, for this series of complexes the trifluoropropynyl ligand is not a particularly impactful candidate for significantly blueshifting emission.

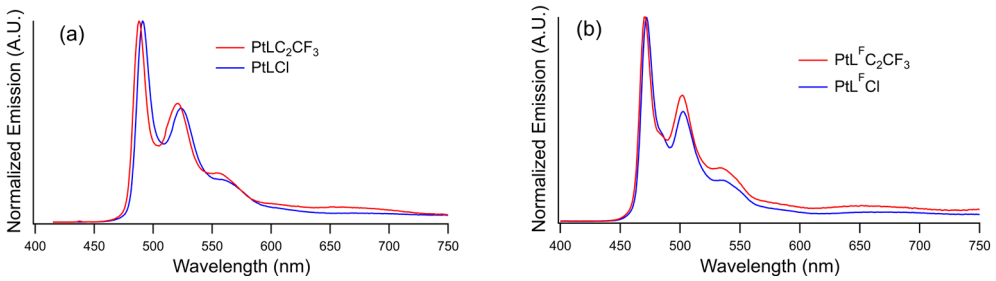

Figure 8. Room-temperature (RT) emission spectra of (**a**) $PtLC_2CF_3$ and PtLCl (λ_{ex} = 392 nm) and (**b**) $PtL^FC_2CF_3$ and PtL^FCl (λ_{ex} = 360 nm) at very low concentrations ([Pt] ≈ 2.0×10^{-6} M) in Ar-purged CH_2Cl_2 solution.

For both complexes, the lowest-energy, spin-forbidden absorption peak (Supplementary Materials, Figure S7) is <10 nm lower in wavelength than the corresponding emission peak. This very small Stokes shift is indicative of an excited state that is relatively undistorted from the ground-state geometry [14]. In addition, there is less than a 5 nm blueshift of the emission in a rigid medium (77 K glass, 1:4 CH_2Cl_2:2-MeTHF) compared to the spectra in solution (Supplementary Materials, Figure S10). This very small rigidochromic shift is also consistent with a relatively undistorted excited state [7].

3.2.3. Computational Investigation

To further investigate the nature of the emissive ESs, time-dependent density functional theory (TDDFT) experiments were performed. Vertical $S_0 \rightarrow T_1$ absorption energies are considered good models for 0-0 emission energies, especially in a rigid medium where structural relaxation has little effect on the emission energy [48,49]. A recent review suggested that density functional theory (DFT) geometry optimization using B3LYP/LANL2DZ followed by TDDFT calculations of the transition from the ^{1}GS to the lowest energy ^{3}ES gave the best predictions for emission energies [50]. Yersin's group also demonstrated that the B3LYP function handled calculations of MLCT and LC excited states well [48]. Finally, our recent benchmarking on a similar set of trifluoropropynyl complexes indicated that for this class of Pt^{II} complexes, TDDFT calculations using

B3LYP/6-31G*/LANL2DZ gave accurate predictions of emission energies and orbital character of the ES [7]. Thus, $PtLC_2CF_3$, PtLCl, $PtL^FC_2CF_3$, and PtL^FCl were modeled using B3LYP/6-31G*/LANL2DZ//B3LYP/LANL2DZ (TDDFT//Geometry-Optimization). All calculations employed a Tomasi polarizable continuum model assigned the dielectric constant for CH_2Cl_2 [51]. There is excellent agreement between the computationally predicted lowest-energy triplet energy and the experimentally determined 0-0 band (77 K glass), suggesting that the computational model utilized is a good fit for simulating these Pt^{II} systems (Table 3).

Table 3. Emission wavelength, TDDFT-calculated $S_0 \rightarrow T_1$ wavelength, and population analysis [a].

Complex	Experimental λ_{PL} [b] (77K)	Predicted λ_{PL} [c]	Pt	Phenyl	Pyridines	X [d]	Orbitals [e]
PtLCl	486 nm	484 nm	32 → 6 (−26)	38 → 26 (−12)	21 → 68 (47)	9 → 0 (−9)	78 → 79 (49%) 77 → 80 (33%)
$PtLC_2CF_3$	483 nm	483 nm	25 → 6 (−19)	43 → 25 (−18)	23 → 67 (44)	9 → 2 (−7)	92 → 93 (47%) 91 → 94 (44%)
PtL^FCl	467 nm	467 nm	30 → 6 (−24)	36 → 27 (−9)	23 → 67 (44)	11 → 0 (−11)	86 → 87 (44%) 85 → 87 (38%)
$PtL^FC_2CF_3$	466 nm	465 nm	23 → 6 (−17)	41 → 27 (−14)	24 → 65 (41)	11 → 2 (−9)	99 → 102 (43%) 100 → 101 (41%)

[a] TDDFT and Mulliken population analysis used the B3LYP/6-31G*/LANL2DZ computational model. All structures were optimized as singlets with the B3LYP/LANL2DZ computational model. Columns 4–7 indicate Mulliken population changes for each molecular region. [b] Wavelength of 0-0 emission band. [c] Computationally predicted energy of the lowest-energy triplet state. [d] X is the non-chelating ligand. [e] Frontier molecular orbitals involved in the transition as depicted in Supplementary Materials, Figure S11.

The population analysis (Table 3) and MO images (Supplementary Materials, Figure S11) are consistent with the character of the emissive excited states assigned based on the spectroscopy, namely that they are of mixed ^{3}ILCT(π-π^*)/^{3}MLCT character. For example, for $PtLC_2CF_3$, the calculations show that for the lowest-energy triplet there is a decrease in electron density at both the platinum and the phenyl rings (19% and 18%, respectively), along with an increase in electron density at the pyridine rings (44%). The same general trend is observed for PtLCl, but importantly, the contribution from the platinum to the pyridine rings (26%) played a more dominant role than the transition from the phenyl to the pyridine rings (12%). This is consistent with the :C≡C–CF_3 ligand acting as more electron-withdrawing than the chloro ligand. The same general observations are true of the corresponding L^F complexes. Note that these CT components account for only half of the electronic transition, indicating a significant amount of localized π-π^* character.

3.2.4. Excimer Formation and Excited-State Kinetics

As the [Pt] is increased to $\geq 1 \times 10^{-5}$ M in the RT CH_2Cl_2 solution, broad, unstructured emission peaks appear for $PtLC_2CF_3$ (668 nm) and $PtL^FC_2CF_3$ (659 nm) that are not significant in more dilute solutions (Figure 9). This same behavior has been observed for the corresponding chloro analogues, PtLCl and PtL^FCl, and is attributed to excimer emission from a ^{3}MMLCT excited state [17,21]. Recall that ground-state aggregation was ruled out by the Beer–Lambert Law plot. Thus, this emission must be the result of the formation of an excimer (excited-state dimer) from a ground-state monomer and an excited-state monomer. In addition, there is a more pronounced blueshift (15–20 nm) of the excimer emission of the :C≡C–CF_3 complexes relative to their corresponding Cl complexes (Figure 9) than for monomer emission. Similar behavior was observed for PtLCl and PtLI, where the more electronegative Cl resulted in a 15 nm blueshift of the excimer emission relative to the iodo complex, whereas there was only a 2 nm blueshift for the monomer emission [19]. This supports the hypothesis that :C≡C–CF_3 is more electron-withdrawing than Cl. This is confirmed by the Mulliken charge distribution obtained from DFT calculations. Chiefly, for PtLX the charge on the Pt increases from +0.457 to +0.890 upon replacement of Cl with :C≡C–CF_3. Likewise, for PtL^FCl the charge on the Pt increases from +0.505 to +0.945. Furthermore, the greater blueshift of the excimer relative to the monomer emission indicates

that the electron density on the X ligand has a greater impact on the HOMO of the excimer (σ^*d_{z2}) than on the HOMO of the monomer (d_{z2}).

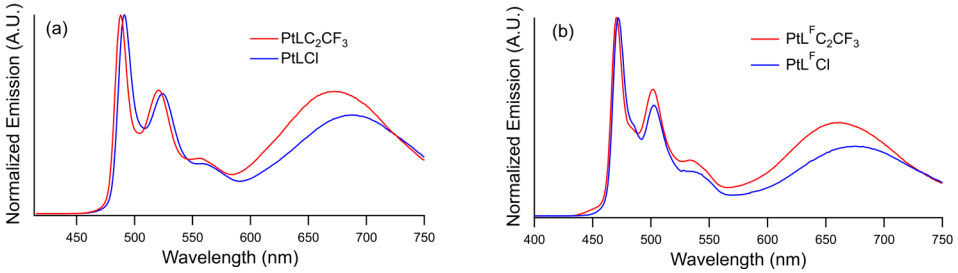

Figure 9. RT emission spectra showing monomer and excimer peaks of (**a**) $PtLC_2CF_3$ and PtLCl at [Pt] = 1.2×10^{-4} M (λ_{ex} = 392 nm) and (**b**) $PtL^FC_2CF_3$ and PtL^FCl (λ_{ex} = 366 nm) at [Pt] = 1.3×10^{-4} M in Ar-purged CH_2Cl_2 solution.

As the [Pt] increases, the intensity of monomer emission decreases while the intensity of excimer emission increases (Supplementary Materials, Figure S12). This is accompanied by a decrease in the quantum yield (Φ_{PL}) and lifetime of monomer emission with increasing platinum concentration. A kinetic scheme proposed by Shinozaki and coworkers for PtLCl and analogous complexes [17,22] is adopted herein (Scheme 1). For some complexes, at even higher concentrations, trimer formation complicates the overall kinetic scheme [17]. Here, k_{sq} represents the rate constant for self-quenching (i.e., the excimer formation rate constant), k_{-sq} is the rate constant for the reverse process, k_M is the intrinsic rate constant of the deactivation of the excited-state monomer in the absence of self-quenching, and k_E is the intrinsic rate constant for the deactivation of the excimer in the absence of contributions from k_{-sq} and trimer formation.

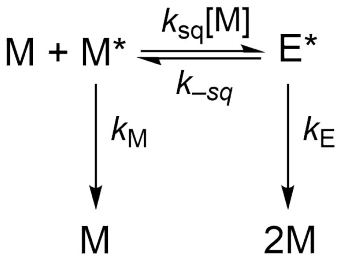

Scheme 1. Kinetic scheme of all relevant paths of deactivation for PtLX complexes in deaerated solution.

Given that both excimer and monomer emission can be observed and are well separated, it is possible to measure the total deactivation rate constant, k_d, at both the monomer emission wavelength (k_{dM}) and the excimer emission wavelength (k_{dE}). At very low concentrations, the equilibrium lies toward M*, and a Stern–Volmer plot based on k_{dM} yields a slope of k_{sq} and an intercept of k_M (Equation (1) and Supplementary Materials, Figure S13). The values for the monomer lifetimes ($\tau_M = 1/k_M$) are determined from the intercept of these plots (Table 4). In addition, the emission quantum yields for the monomer

$$k_{dM} = k_{sq}[Pt] + k_M \quad (1)$$

were measured at concentrations where self-quenching is negligible. Lastly, the emission is quenched in the presence of oxygen. The relevant lifetimes and quantum yields for the C_2CF_3 complexes in deaerated and air-saturated solutions reported herein are compared to those of the analogous Cl complexes reported in the literature. Perhaps the most unexpected result is that the photoluminescence quantum yield for $PtL^FC_2CF_3$ in deaerated solution is around a quarter of that for the corresponding Cl complex, whereas the corresponding

lifetimes differ by only a factor of two. Measurements on different samples and repeated purifications of the complex did not result in a change in Φ_{PL}; thus, we believe this lower quantum yield is not due to a quenching impurity, but rather an increase in the non-radiative rate constant along with a decrease in the radiative rate constant for this complex. We do not currently have an explanation for this difference.

Table 4. Photophysical constants of Pt(N^C^N) complexes in CH_2Cl_2.

Compound	Emission RT		QY_{lum}		τ_M	
	Monomer λmax	Excimer λmax	Ar	Air	Ar	Air
PtLCl [a]	491	691	0.60	0.04	7.2	0.5
$PtLC_2CF_3$	487	668	0.53 [b]	0.061 [b]	7.1 [c]	0.8 [c]
PtL^FCl [a]	472	677	0.85	0.09	7.9	0.7
$PtL^FC_2CF_3$	471	659	0.22 [b]	0.062 [b]	4.2 [c]	0.9 [c]

[a] Reference 20. [b] Calculated relative quantum yield value using quinine hemisulfate monohydrate in 0.1 M H_2SO_4 as a standard. Absorbances were matched at 360 nm for [Pt] ≈ 2.5×10^{-6} M. [c] The k_{dM} of Pt solns was plotted against [Pt] over a range of conc. from ≈5.0×10^{-6} M to ≈2.5×10^{-5} M. τ_M is the inverse of k_M, which is the y-intercept.

WOLED applications depend on controlling the excimer-to-monomer emission intensity ratio to achieve white emission. Thus, we investigated whether the trifluoropropynyl ligand impacts this ratio relative to the chloro ligand. A strict comparison requires that corresponding emission spectra must be collected under conditions where both the initial ground-state and excited-state concentrations of the Pt monomer ([M] and [M*], respectively; Scheme 1) are identical. This requires absorbance-matching solutions of the complexes at wavelengths where the two complexes have identical molar absorptivities, followed by excitation at that wavelength. The spectra in Figure 9 are indeed performed under these conditions, and then normalized at the maximum emission intensity of the monomer in order to show the relative monomer/excimer emission. Clearly, the trifluoropropynyl ligand increases the relative intensity of the excimer emission and may indicate that the trifluoropropynyl ligand increases the equilibrium constant for excimer formation.

3.3. Emission in PMMA Film

Details relevant to excited-state reorganization and possible use in OLED devices can be gained from the investigation of emission in films. Thus, the emission in PMMA films of $PtLC_2CF_3$ and $PtL^FC_2CF_3$ were investigated and compared to emission in solution (Supplementary Materials, Figure S14). For $PtLC_2CF_3$, the monomer emission in the RT PMMA film is nearly identical to that in the RT CH_2Cl_2 solution (λ_{max} = 487 and 488 nm, respectively). Likewise, for $PtL^FC_2CF_3$, λ_{max} = 470 nm in both media. The fine structure is also unaffected by this change in medium. This lack of rigidochromic behavior is consistent with the conclusion that the excited-state geometry of the monomer is close to the ground-state geometry [7,52–56], and has been reported for PtL^FCl [57,58] and other similar Pt^{II} complexes [8,36,37].

The excimer emission peaks, on the other hand, show significant rigidochromic behavior. For example, $PtLC_2CF_3$ (650 nm) and $PtL^FC_2CF_3$ (641 nm) in PMMA film are both blueshifted by 18 nm relative to those in CH_2Cl_2 solution (668 nm and 659 nm, respectively; Supplementary Materials, Figure S14). This rigidochromic shift of the excimer emission suggests that the geometry of the excimer may be significantly distorted from the geometry of the corresponding ground-state dimer. A similar rigidochromic shift in excimer emission has been reported for PtL^FCl [57,58] and a spiro-flourine-chelated Pt^{II} complex [59], which both emit from ^{3}MMLCT excited states. Additionally, the Castellano group reported solution-phase calculations of a 0.19 Å shortening of the Pt---Pt bond of the excimer when compared to the corresponding ground-state dimer [44]. Such distortion is likely inhibited in film. Therefore, the observed rigidochromic blueshift is consistent with the classification

of the emissive ^{3}ES of the excimer as a ^{3}MMLCT state and this blueshift may be explained by the inhibition of the Pt---Pt bond contraction in film.

A single-component WOLED device using a film of 8% (*w*/*w*) PtL^{F}Cl with notably white CIE chromaticity coordinates (0.33, 0.35) has been reported [58]. Thus, attempts were made to prepare films of PtL^{F}C$_2$CF$_3$ at 8% Pt *w*/*w*. However, the C$_2$CF$_3$ complexes proved to be insoluble at the [Pt] concentrations required for solution processing of 8% Pt *w*/*w* film. Therefore, films were prepared at lower [Pt] concentrations. A PMMA film of PtL^{F}C$_2$CF$_3$ (0.7% Pt *w*/*w*) showing a good balance of both monomer and excimer emission resulting in a warm orange-white emission with CIE chromaticity coordinates of (0.39, 0.38) was prepared and characterized (Figure 10). At that same concentration of [Pt] (0.7% Pt *w*/*w*), PtL^{F}Cl exhibits very little excimer emission. Further, in films at greater concentrations that typify OLED devices, the perceived color of emission from PtLC$_2$CF$_3$ and PtL^{F}C$_2$CF$_3$ grows redder at such a magnitude as to render the C$_2$CF$_3$ complexes ineffective for WOLED devices.

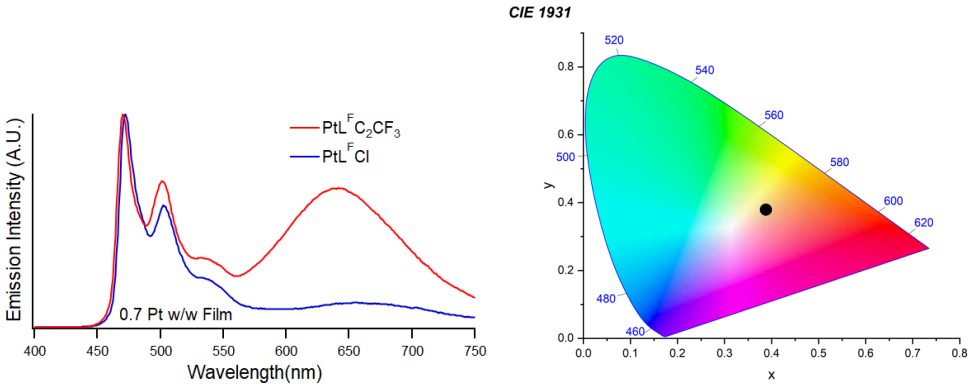

Figure 10. RT emission spectra of 0.7% Pt w/w PMMA films of PtL^{F}Cl and PtL^{F}C$_2$CF$_3$ and CIE 1931 *xy* chromaticity diagram showing the chromaticity coordinates (black dot) for the PtL^{F}C$_2$CF$_3$ film.

3.4. Oxygen Quenching

As [O$_2$] increases in the RT CH$_2$Cl$_2$ solution, the intensity of the emission spectra of PtLCl, PtLC$_2$CF$_3$, PtL^{F}Cl, and PtL^{F}C$_2$CF$_3$ decreases due to quenching by energy transfer. This has previously been reported for monomer emission for PtLCl and PtL^{F}Cl as well as other similar Pt^{II} complexes [20,21,60,61]. It is noteworthy that the excimer emission is quenched by oxygen to a larger extent than the monomer in the RT CH$_2$Cl$_2$ solution (Figures 11 and 12). This is particularly evident in spectra where the monomer emission has been normalized (Figure 12).

In order to probe the suitability of this class of Pt^{II} complexes as ratiometric sensors of [O$_2$], the ratio of the peak intensity of the excimer to that of the monomer, I_E/I_M, was plotted against the concentration of oxygen in CH$_2$Cl$_2$ solutions (Figure 13). Three [O$_2$] values were used: 0 M (Ar-purged), 2.2×10^{-3} M (air-saturated), and 1.07×10^{-2} M (O$_2$-purged) [62]. Similar behavior was observed for all complexes investigated herein. A greater change in I_E/I_M occurs between Ar-purged and air-saturated solutions than between air-saturated and oxygen-saturated solutions. This suggests that the emission ratios of these complexes are more sensitive to changes in [O$_2$] under hypoxic conditions.

The conditions under which such complexes demonstrate the greatest change in excimer/monomer emission ratio were further evaluated using PtL^{F}Cl and PtL^{F}C$_2$CF$_3$ test cases. To achieve this, the factor of increase in the excimer/monomer ratio (Equation (2)) between Ar- and air-saturated solutions was used as a gauge of sensitivity and was plotted against either excitation wavelength or [Pt] concentration. Whereas there was no observable impact of excitation wavelength across the range from 300 to 375 nm for either PtL^{F}Cl or PtL^{F}C$_2$CF$_3$ (Supplementary Materials, Figure S15), there was a significant dependence on concentration, with the sensitivity going through a maximum at ≈30 μM for PtL^{F}C$_2$CF$_3$ (Figure 14) with a similar trend observed for PtL^{F}Cl (Supplementary Materials, Figure S16).

Such concentrations provide a good balance of excimer to monomer emission in the absence of oxygen. Significantly higher [Pt] concentrations are dominated by the excimer and significantly lower concentrations are dominated by the monomer, lowering the sensitivity.

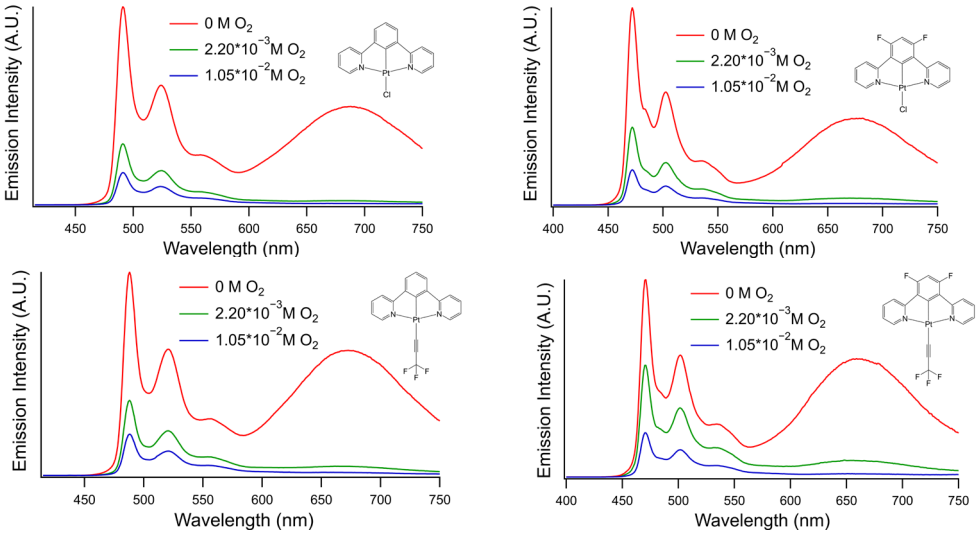

Figure 11. Emission spectra of platinum complexes in Ar-purged (0 M O_2), air-saturated (2.2×10^{-3} M O_2), and O_2-purged (1.07×10^{-2} M O_2) RT CH_2Cl_2 solutions at high Pt concentrations ([Pt] = 1.0×10^{-4} M). Solutions of PtLX complexes are absorbance-matched at λ_{ex} = 392 nm, and solutions of PtL^FX complexes are absorbance-matched at λ_{ex} = 360 nm.

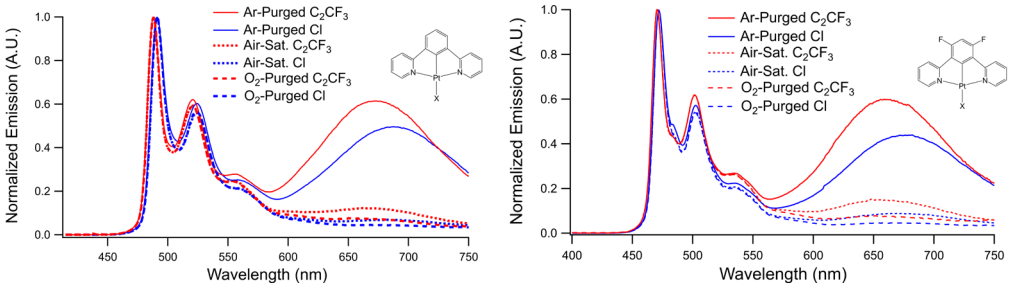

Figure 12. Emission spectra of platinum complexes in Ar-purged, air-saturated, and O_2-purged RT CH_2Cl_2 solutions ([Pt] = 1.0×10^{-4} M). Solutions of PtLX complexes are absorbance-matched at λ_{ex} = 392 nm, and solutions of PtL^FX complexes are absorbance-matched at λ_{ex} = 360 nm.

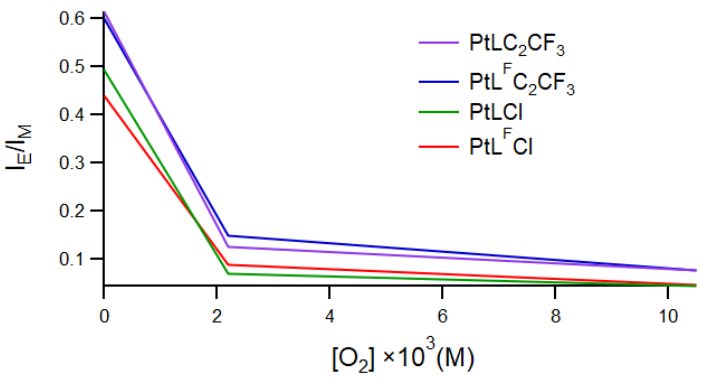

Figure 13. Plots of excimer-to-monomer emission ratios in RT CH_2Cl_2 solutions ([Pt] = 1.2×10^{-4} M), as a function of [O_2] (0 M O_2, 2.2×10^{-3} M O_2, and 1.07×10^{-2} M O_2). Solutions of PtLX complexes are absorbance-matched at λ_{ex} = 392 nm, and solutions of PtL^FX complexes are absorbance-matched at λ_{ex} = 360 nm.

$$E/M\text{Factor of Increase} = \frac{(I_E/I_M)_{Ar}}{(I_E/I_M)_{air}}. \quad (2)$$

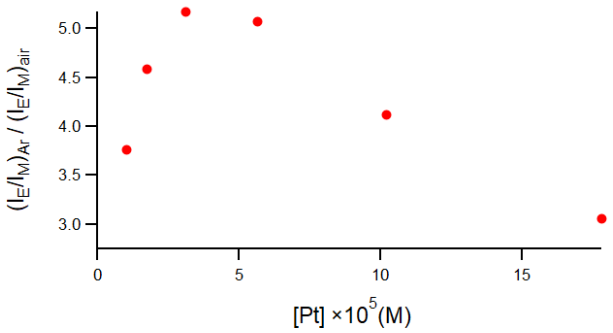

Figure 14. Plot of the quotients of the excimer/monomer emission ratios of Ar-purged (0 M O_2) solution over air-saturated (2.2×10^{-3} M O_2) solution for $PtL^FC_2CF_3$ at different [Pt] concentrations in RT CH_2Cl_2 solution (λ_{ex} = 360 nm).

It is noteworthy that a differential dependence of monomer vs. excimer emission intensity on oxygen concentration requires that equilibrium between the excited monomer and excimer not be rapidly maintained under these conditions. This is indeed the case, as demonstrated by the following analysis. If the excimer/monomer equilibrium were rapid under all conditions, then the apparent deactivation rate constants for monomer and excimer k_{dM} and k_{dE} would be equal under all conditions. Using $PtL^FC_2CF_3$ as an example, we have observed that deaerated CH_2Cl_2 solutions at ~5×10^{-5} M have a k_{dM} (3.95×10^5 s^{-1}) that is 19% greater than the k_{dE} (3.31×10^5 s^{-1}). However, whereas both rate constants increase with an increase in concentration (Table S3), they do so with different slopes such that at [Pt] ≈ 1×10^{-3} M, k_{dE} (2.54×10^6 s^{-1}) is only half of the value for k_{dM} (4.95×10^6 s^{-1}). This same trend is observed for $PtLC_2CF_3$ (Supplementary Materials, Table S5). This suggests that equilibrium is not rapid relative to excited-state deactivation, in agreement with reports that $k_{-sq} < k_E$ for a range of similar Pt^{II} complexes [17,19,22,23], and given that the monomer/excimer equilibrium is not rapid in the absence of oxygen, the presence of oxygen would only exacerbate this. Chiefly, the rate constants for the establishment of equilibrium (k_{sq}, and k_{-sq}) are independent of [O_2], but the deactivation rate constants of both the monomer and excimer increase in the presence of oxygen.

4. Conclusions

The trifluoropropynyl ligand was investigated for its impact on the structure and emission characteristics of Pt complexes of two NˆCˆN ligands. Namely, the trifluoropropynyl complexes were compared with their chloro analogues. There was a slight increase in the Pt-C_{NCN} bond length for the trifluoropropynyl complex vs. the chloro complex; otherwise, the structures were largely similar. The chief reason for replacing the Cl ligand with the trifluoropropynyl ligand was to attempt to blueshift the monomer emission for potential OLED use as a blue emitter, or for WOLED use. The <4 nm blueshift of the monomer, and the propensity for $PtL^FC_2CF_3$ to form excimers at a lower concentration, suggests that these complexes are not useful in either of these applications. However, it was observed during these investigations that for both the Cl and :C≡C–CF_3 complexes, there was a differential sensitivity of the monomer and excimer emission to oxygen, raising the possibility that these and other related Pt complexes that show excimer emission might be useful in ratiometric oxygen sensors. Clearly, to be used in a device, these complexes would need to be suspended in an oxygen-permeable rigid substrate as has been carried out in sol–gel for Pt-porphyrin complexes [63–66], but these gels rely on an additional doped reference dye, and thus become less accurate over time as the Pt-porphyrin degrades. Avoiding this issue, ratiometric oxygen sensors that rely solely on singlet and triplet emission from

[(dppe)Pt{$S_2C_2(CH_2CH_2$–N–2-pyridinium)}](BPh_4)] have been manufactured in cellulose acetate film [67,68]. Thus, further research into the oxygen sensitivity of excimer and monomer emission from NˆCˆN-chelated Pt^{II} complexes in cellulose–acetate films will be helpful in determining the suitability of these complexes to ratiometric oxygen-sensing applications.

Supplementary Materials: The following supporting information can be downloaded at https://www.mdpi.com/article/10.3390/cryst14080678/s1: Figure S1: ^{1}H-NMR spectrum of $PtLC_2CF_3$ in DMSO-d_6, Figure S2: ^{1}H-NMR spectrum of $PtL^FC_2CF_3$ in $CDCl_3$, Figure S3: Selected intermolecular interactions in the $PtLC_2CF_3$ complex, Figure S4: Selected intermolecular interactions in the $PtL^FC_2CF_3$ complex, Figure S5: Additional unit-cell packing diagrams for $PtLC_2CF_3$, Figure S6: Additional unit-cell packing diagrams for $PtL^FC_2CF_3$, Table S1: Selected bond lengths and angles in $PtLC_2CF_3$, Table S2: Selected bond lengths and angles in $PtL^FC_2CF_3$, Table S3: Wavelengths and Molar Absorptivities of Absorbance Peaks of Cl and C_2CF_3 complexes, Figure S7: Overlay of spin-forbidden absorption peaks of $PtLC_2CF_3$ and $PtL^FC_2CF_3$, Figure S8: Beer's Law Plots of $PtLC_2CF_3$ and $PtL^FC_2CF_3$, Table S4: Wavelengths and Frequencies of, and Changes in Frequency between, Emission Peaks of $PtLC_2CF_3$ and $PtL^FC_2CF_3$, Figure S9: Overlay of Absorption and Excitation spectra of $PtLC_2CF_3$ and $PtL^FC_2CF_3$, Figure S10: Overlay of Emission Spectra of $PtLC_2CF_3$ and $PtL^FC_2CF_3$ at RT and 77K, Figure S11: Ball and Stick Models of Computationally Predicted Molecular Orbitals, Figure S12: Overlay of emission spectra of PtL^FCl at various [Pt], Figure S13: Modified Stern–Volmer plots of k_d vs. [Pt] for $PtLC_2CF_3$ and $PtL^FC_2CF_3$ to find k_{sq} and k_M, Figure S14: Overlay of PMMA film and CH_2Cl_2 solution emission spectra of $PtLC_2CF_3$ and $PtL^FC_2CF_3$, Figure S15: Plots of factor of increase in Excimer/Monomer emission ratio between Ar-purged and air-saturated solutions vs. excitation wavelength for PtL^FCl and $PtL^FC_2CF_3$, Figure S16: Plot of factor of increase in Excimer/Monomer emission ratio between Ar-purged and air-saturated solutions vs. [Pt] for PtL^FCl, Table S5: k_{dM} and k_{dE} of $PtLC_2CF_3$ at various [Pt].

Author Contributions: Conceptualization, J.H.Z., J.S.M. and P.S.W.; methodology, J.H.Z., P.S.W. and C.D.M.; validation, J.H.Z., B.J.C., W.M.T. and C.D.M.; formal analysis, J.H.Z., B.J.C., W.M.T., C.D.M. and P.S.W.; investigation, J.H.Z., B.J.C., W.M.T., J.S.M. and C.D.M.; resources, P.S.W. and C.D.M.; data curation, J.H.Z., C.D.M. and P.S.W.; writing—original draft preparation, J.H.Z., C.D.M. and P.S.W.; writing—review and editing, J.H.Z., B.J.C., W.M.T., J.S.M., C.D.M. and P.S.W.; visualization, J.H.Z., B.J.C., W.M.T., C.D.M. and P.S.W.; supervision, P.S.W. and C.D.M.; project administration, P.S.W. All authors have read and agreed to the published version of the manuscript.

Funding: Support is acknowledged from the National Science Foundation under Grant No. 2055326. Any opinions, findings, and conclusions or recommendations expressed in this material are those of the authors and do not necessarily reflect those of the National Science Foundation.

Data Availability Statement: CCDC 2364563-2364564 contain the supplementary crystallographic data for this paper. These data can be obtained from the CCDC, 12 Union Road, Cambridge CB2 1EZ, UK; Fax: +44-1223-336033.

Conflicts of Interest: The authors declare no conflicts of interest.

References

1. Koziar, J.C.; Cowan, D.O. Photochemical Heavy-Atom Effects. *Acc. Chem. Res.* **1978**, *11*, 334–341. [CrossRef]
2. Gildea, L.F.; Williams, J.A.G. 3—Iridium and platinum complexes for OLEDs. In *Organic Light-Emitting Diodes (OLEDs): Materials, Devices, and Applications*; Buckley, A., Ed.; Woodhead Publishing Series in Electronic and Optical Materials; Woodhead Publishing: Sawston, UK, 2013; pp. 77–113.
3. Li, X.; Zhang, J.; Zhao, Z.; Wang, L.; Yang, H.; Chang, Q.; Jiang, N.; Liu, Z.; Bian, Z.; Liu, W.; et al. Deep Blue Phosphorescent Organic Light-Emitting Diodes with CIEy Value of 0.11 and External Quantum Efficiency up to 22.5%. *Adv. Matter.* **2018**, *30*, 1705005. [CrossRef] [PubMed]
4. Bullock, J.D.; Valandro, S.R.; Sulicz, A.N.; Zeman, C.J.; Abboud, K.A.; Schanze, K.S. Blue Phosphorescent trans-N-Heterocyclic Carbene Platinum Acetylides: Dependence on Energy Gap and Conformation. *J. Phys. Chem. A* **2019**, *123*, 9069–9078. [CrossRef] [PubMed]
5. Kido, J.; Kimura, M.; Nagai, K. Multilayer White Light-Emitting Organic Electroluminescent Device. *Science* **1995**, *267*, 1332–1334. [CrossRef] [PubMed]
6. Reineke, S.; Lindner, F.; Schwartz, G.; Seidler, N.; Walzer, K.; Lüssem, B.; Leo, K. White organic light-emitting diodes with fluorescent tube efficiency. *Nature* **2009**, *459*, 234–238. [CrossRef] [PubMed]

7. McCarthy, J.S.; McCormick, M.J.; Zimmerman, J.H.; Hambrick, H.R.; Thomas, W.M.; McMillen, C.D.; Wagenknecht, P.S. Role of the Trifluoropropynyl Ligand in Blue-Shifting Charge-Transfer States in Emissive Pt Diimine Complexes and an Investigation into the PMMA-Imposed Rigidoluminescence and Rigidochromism. *Inorg. Chem.* **2022**, *61*, 11366–11376. [CrossRef] [PubMed]
8. Lu, W.; Chan, M.C.W.; Zhu, N.; Che, C.M.; He, Z.; Wong, K.Y. Structural Basis for Vapoluminescent Organoplatinum Materials Derived from Noncovalent Interactions as Recognition Components. *Chem. Eur. J.* **2003**, *9*, 6155–6166. [CrossRef] [PubMed]
9. Lu, W.; Mi, B.X.; Chan, M.C.W.; Hui, Z.; Che, C.M.; Zhu, N.; Lee, S.T. Light-Emitting Tridentate Cyclometalated Platinum(II) Complexes Containing σ-Alkynyl Auxiliaries: Tuning of Photo- and Electrophosphorescence. *J. Am. Chem. Soc.* **2004**, *126*, 4958–4971. [CrossRef] [PubMed]
10. Chow, P.K.; To, W.P.; Low, K.H.; Che, C.M. Luminescent Palladium(II) Complexes with π-Extended Cyclometalated [R−C^N^N-R′] and Pentafluorophenylacetylide Ligands: Spectroscopic, Photophysical, and Photochemical Properties. *Chem. Asian J.* **2014**, *9*, 534–545. [CrossRef]
11. Rossi, E.; Colombo, A.; Dragonetti, C.; Righetto, S.; Roberto, D.; Ugo, R.; Valore, A.; Williams, J.A.G.; Lobello, M.G.; De Angelis, F.; et al. Tuning the Dipolar Second-Order Nonlinear Optical Properties of Cyclometalated Platinum(II) Complexes with Tridentate N^C^N Binding Ligands. *Chem. Eur. J.* **2013**, *19*, 9875–9883. [CrossRef]
12. Mcdarmont, S.L.; McCormick, M.J.; Wagenknecht, P.S.; Duplooy, L.E.; Pienkos, J.A.; McMillen, C.D. The Synthesis and Crystallographic Characterization of Emissive Pt(II) and Au(I) Compounds Exploiting the 2-Ethynylpyrimidine Ligand. *Crystals* **2024**, *14*, 587. [CrossRef]
13. Rausch, A.F.; Murphy, L.; Williams, J.A.G.; Yersin, H. Improving the performance of Pt(II) complexes for blue light emission by enhancing the molecular rigidity. *Inorg. Chem.* **2012**, *51*, 312–319. [CrossRef] [PubMed]
14. Wagenknecht, P.S.; Ford, P.C. Metal Centered Ligand Field Excited States: Their Roles in the Design and Performance of Transition Metal Based Photochemical Molecular Devices. *Coord. Chem. Rev.* **2011**, *255*, 591–616. [CrossRef]
15. Williams, J.A.G. Platinum. In *Photochemistry and Photophysics of Coordination Compounds II*; Springer: Berlin/Heidelberg, Germany, 2007; pp. 205–268.
16. Eddy, L.E.; Thakker, P.U.; McMillen, C.D.; Pienkos, J.A.; Cordoba, J.J.; Edmunds, C.E.; Wagenknecht, P.S. A comparison of the metal-ligand interactions of the pentafluorophenylethynyl and trifluoropropynyl ligands in transition metal cyclam complexes. *Inorg. Chim. Acta* **2019**, *486*, 141–149. [CrossRef]
17. Kayano, T.; Takayasu, S.; Sato, K.; Shinozaki, K. Luminescence Color Tuning of Pt^{II} Complexes and a Kinetic Study of Trimer Formation in the Photoexcited State. *Chem. Eur. J.* **2014**, *20*, 16583–16589. [CrossRef] [PubMed]
18. Sun, C.; Thakker, P.U.; Khulordava, L.; Tobben, D.J.; Greenstein, S.M.; Grisenti, D.L.; Kantor, A.G.; Wagenknecht, P.S. Trifluoropropynyl as a Surrogate for the Cyano Ligand and Intense, Room-Temperature, Metal-Centered Emission from Its Rh(III) Complex. *Inorg. Chem.* **2012**, *51*, 10477–10479. [CrossRef] [PubMed]
19. Iwakiri, A.; Konno, Y.; Shinozaki, K. Determination of excimer emission quantum yield of Pt(dpb)Cl (dpbH = 1, 3-di(2-pyridyl)benzene and its analogues in solution). *J. Lumin.* **2019**, *207*, 482–490. [CrossRef]
20. Rossi, E.; Murphy, L.; Brothwood, P.L.; Colombo, A.; Dragonetti, C.; Roberto, D.; Ugo, R.; Cocchi, M.; Williams, J.A.G. Cyclometallated platinum(II) complexes of 1,3-di(2-pyridyl)benzenes: Tuning excimer emission from red to near-infrared for NIR-OLEDs. *J. Mater. Chem.* **2011**, *21*, 15501–15510. [CrossRef]
21. Williams, J.A.G.; Beeby, A.; Davies, E.S.; Weinstein, J.A.; Wilson, C. An Alternative Route to Highly Luminescent Platinum(II) Complexes: Cyclometalation with N^C^N-Coordinating Dipyridylbenzene Ligands. *Inorg. Chem.* **2003**, *42*, 8609–8611. [CrossRef] [PubMed]
22. Hattori, S.; Nakano, T.; Nakano, K.; Konno, Y.; Nishibori, E.; Galica, T.; Shinozaki, K. Luminescence color change of [3,4-difluoro-2,6-bis(5-methyl-2-pyridyl)phenyl-κ3N,C1,N′]cyanidoplatinum(II) by aggregation. *Dalton Trans.* **2022**, *51*, 15830. [CrossRef]
23. Watanabe, H.; Iwamura, M.; Nozaki, K. Kinetic Analysis of Excited-State Dynamics of Emissive Oligomers of Pt(II) Complex in Solution. *Inorg. Chem.* **2024**, *63*, 5580–5585. [CrossRef] [PubMed]
24. Lee, W.W.S.; Wong, K.Y.; Li, X.M. Luminescent Dicyanoplatinum(II) Complexes as Sensors for the Optical Measurement of Oxygen Concentrations. *Anal. Chem.* **1993**, *65*, 255–258. [CrossRef]
25. Cárdenas, D.J.; Echavarren, A.M.; Ramírez de Arellano, M.C. Divergent Behavior of Palladium(II) and Platinum(II) in the Metalation of 1,3-Di(2-pyridyl)Benzene. *Organometallics* **1999**, *18*, 3337–3341. [CrossRef]
26. Wang, Z.; Turner, E.; Mahoney, V.; Madakuni, S.; Groy, T.; Li, J. Facile synthesis and Characterization of Phosphorescent Pt(N^CF_2^N)X Complexes. *Inorg. Chem.* **2019**, *49*, 11276–11286. [CrossRef] [PubMed]
27. *APEX 3*, Version 2017.3; Bruker-AXS Inc.: Madison, WI, USA, 2017.
28. Sheldrick, G.M. SHELXT—Integrated space-group and crystal-structure determination. *Acta Crystallogr. Sect. A Found. Adv.* **2015**, *71*, 3–8. [CrossRef] [PubMed]
29. Sheldrick, G.M. Crystal structure refinement with SHELXL. *Acta Crystallogr. Sect. C Struct. Chem.* **2015**, *71*, 3–8. [CrossRef] [PubMed]
30. Frisch, M.J.; Trucks, G.W.; Schlegel, H.B.; Scuseria, G.E.; Robb, M.A.; Cheeseman, J.R.; Scalmani, G.; Barone, V.; Petersson, G.A.; Nakatsuji, H.; et al. *Gaussian 16*, Revision C.01; Gaussian Inc.: Wallingford, CT, USA, 2016.
31. Becke, A.D. Density-functional exchange-energy approximation with correct asymptotic behavior. *Phys. Rev. A At. Mol. Opt. Phys.* **1988**, *38*, 3098–3100. [CrossRef] [PubMed]

32. Rassolov, V.A.; Ratner, M.A.; Pople, J.A.; Redfern, P.C.; Curtiss, L.A. 6-31G* Basis Set for Third-Row Atoms. *J. Comput. Chem.* **2001**, *22*, 976–984. [CrossRef]
33. Dunning, T.H.; Hay, P.J. *Modern Theoretical Chemistry*; Schaefer, H.F., Ed.; Plenum: New York, NY, USA, 1977; Volume 3, pp. 1–28.
34. Dennington, R.; Keith, T.A.; Millam, J.M. *GaussView*, Version 6; Semichem Inc.: Shawnee Mission, KS, USA, 2016.
35. O'Boyle, N.M.; Tenderholt, A.L.; Langner, K.M. A library for package-independent computational chemistry algorithms. *J. Comp. Chem.* **2008**, *29*, 839–845. [CrossRef]
36. Sonogashira, K.; Fujikura, Y.; Yatake, T.; Toyoshima, N.; Takahashi, S.; Hagihara, N. Synthesis and properties of cis- and trans-dialkynyl complexes of platinum(II). *J. Orgenomet. Chem.* **1978**, *145*, 101–108. [CrossRef]
37. Hissler, M.; Connick, W.B.; Geiger, D.K.; McGarrah, J.E.; Lipa, D.; Lachicotte, R.J.; Eisenberg, R. Platinum Diimine Bis(acetylide) Complexes: Synthesis, Characterization, and Luminescence Properties. *Inorg. Chem.* **2000**, *39*, 447–457. [CrossRef] [PubMed]
38. Chen, Y.; Li, K.; Lu, W.; Chui, S.; Ma, C.-W.; Che, C.-M. Photoresponsive Supramolecular Organometallic Nanosheets Induced by $Pt^{II}\cdots Pt^{II}$ and C–H$\cdots$p Interactions. *Angew. Chem. Int. Ed.* **2009**, *48*, 9909–9913. [CrossRef] [PubMed]
39. Li, B.; Li, Y.; Chan, M.H.-Y.; Yam, V.W.-W. Phosphorescent Cyclometalated Platinum(II) Enantiomers with Circularly Polarized Luminescence Properties and Their Assembly Behaviors. *J. Am. Chem. Soc.* **2021**, *143*, 21676–21684. [CrossRef] [PubMed]
40. Brisdon, A.K.; Crossley, I.R.; Pritchard, R.G. Asymmetric Fluoro-alkynyl Mercurials: The Synthesis and Solid State Structures of RHgC$\dot{:}$CCF$_3$ (R = Ph, Fc). *Organometallics* **2005**, *24*, 5487–5490. [CrossRef]
41. Lin, J.; Zou, C.; Zhang, X.; Gao, Q.; Suo, S.; Shuo, Q.; Chang, X.; Xie, M.; Lu, W. Highly phosphorescent organopalladium(II) complexes with metal-metal-to-ligand charge-transfer excited states in fluid solutions. *Dalton Trans.* **2019**, *48*, 10417–10421. [CrossRef] [PubMed]
42. Poater, A.; Moradell, S.; Pinilla, E.; Poater, J.; Sola, M.; Martínez, M.A.; Llobet, A. A trinuclear Pt(II) compound with short Pt-Pt-Pt contacts. An analysis of the influence of π-π stacking interactions on the strength and length of the Pt-Pt bond. *Dalton Trans.* **2006**, 1188–1196. [CrossRef] [PubMed]
43. Chakraborty, S.; Aliprandi, A.; De Cola, L. Multinuclear Pt^{II} Complexes: Why Three is Better than Two to Enhance Photophysical Properties. *Chem. Eur. J.* **2020**, *26*, 11007–11012. [CrossRef] [PubMed]
44. Roy, S.; Lopez, A.A.; Yarnell, J.E.; Castellano, F.N. Metal−Metal-to-Ligand Charge Transfer in Pt(II) Dimers Bridged by Pyridyl and Quinoline Thiols. *Inorg. Chem.* **2022**, *61*, 121–130. [CrossRef] [PubMed]
45. Wan, K.-T.; Che, C.-M.; Cho, K.-C. Inorganic excimer. Spectroscopy, photoredox properties and excimeric emission of dicyano(4,4-di-tert-butyl-2,2-bipyridine) platinum(II). *Dalton Trans.* **1991**, *4*, 1077–1080. [CrossRef]
46. Brooks, J.; Babayan, Y.; Lamansky, S.; Djurovich, P.I.; Tsyba, I.; Bau, R.; Thompson, M.E. Synthesis and Characterization of Phosphorescent Cyclometalated Platinum Complexes. *Inorg. Chem.* **2002**, *41*, 3055–3066. [CrossRef]
47. Crosby, G.A. Spectroscopic Investigations of Excited States of Transition-Metal Complexes. *Acc. Chem. Res.* **1975**, *8*, 231–238. [CrossRef]
48. Niehaus, T.A.; Hofbeck, T.; Yersin, H. Charge-transfer excited states in phosphorescent organo-transition metal compounds: A difficult case for time dependent density functional theory? *RSC Adv.* **2015**, *5*, 63318–63329. [CrossRef]
49. London, H.C.; Whittemore, T.J.; Gale, A.G.; McMillen, C.D.; Pritchett, D.Y.; Myers, A.R.; Thomas, H.D.; Shields, G.C.; Wagenknecht, P.S. Ligand-to-Metal Charge-Transfer Photophysics and Photochemistry of Emissive d^0 Titanocenes: A Spectroscopic and Computational Investigation. *Inorg. Chem.* **2021**, *60*, 14399–14409. [CrossRef]
50. Morello, G.R. Accurate Prediction of Emission Energies with TD-DFT Methods for Platinum and Iridium OLED Materials. *J. Mol. Model.* **2017**, *23*, 174. [CrossRef]
51. Tomasi, J.; Mennucci, B.; Cammi, R. Quantum Mechanical Continuum Solvation Models. *Chem. Rev.* **2005**, *105*, 2999–3093. [CrossRef] [PubMed]
52. Pomestchenko, I.E.; Castellano, F.N. Solvent Switching between Charge Transfer and Intraligand Excited States in a Multichromophoric Platinum(II) Complex. *J. Phys. Chem. A* **2004**, *108*, 3485–3492. [CrossRef]
53. Whittle, C.E.; Weinstein, J.A.; George, M.W.; Schanze, K.S. Photophysics of Diimine Platinum(II) Bis-Acetylide Complexes. *Inorg. Chem.* **2001**, *40*, 4053–4062. [CrossRef]
54. Chen, P.; Meyer, T.J. Medium Effects on Charge Transfer in Metal Complexes. *Chem. Rev.* **1998**, *98*, 1439–1478. [CrossRef]
55. Chen, P.; Meyer, T.J. Electron Transfer in Frozen Media. *Inorg. Chem.* **1996**, *35*, 5520–5524. [CrossRef]
56. Kozik, M.; Sutin, N.; Winkler, J.R. Energetics and dynamics of solvent reorganization in charge-transfer excited states. *Coord. Chem. Rev.* **1990**, *97*, 23–34. [CrossRef]
57. Fleetham, T.; Ecton, J.; Wang, Z.; Bakken, N.; Li, J. Single-Doped White Organic Light-Emitting Device with an External Quantum Efficiency Over 20%. *Adv. Mater.* **2013**, *25*, 2573–2576. [CrossRef] [PubMed]
58. Yang, X.; Wang, Z.; Madakuni, S.; Li, J.; Jabbour, G.E. Efficient Blue- and White-Emitting Electrophosphorescent Devices Based on Platinum(II)[1,3-Difluoro-4,6-di(2-pyridinyl)benzene] Chloride. *Adv. Mater.* **2008**, *20*, 2405–2409. [CrossRef]
59. Pander, P.; Zaystev, A.V.; Franca, G.L.; Dias, F.B.; Kozhevnikov, V.N. Unusual Excimer/Dimer Behavior of a Highly Soluble C,N Platinum(II) Complex with a Spiro-Fluorene Motif. *Inorg. Chem.* **2023**, *62*, 18465–18473. [CrossRef] [PubMed]
60. Evans, R.C.; Douglas, P.; Williams, J.A.G.; Rochester, D.L. A Novel Luminescence-Based Colorimetric Oxygen Sensor with a "Traffic Light" Response. *J. Fluoresc.* **2006**, *16*, 2. [CrossRef] [PubMed]

61. Farley, S.J.; Rochester, D.L.; Thompson, A.L.; Howard, J.A.K.; Williams, J.A.G. Controlling Emission Energy, Self-Quenching, and Excimer Formation in Highly Luminescent N^C^N-Coordinated Platinum(II) Complexes. *Inorg. Chem.* **2005**, *44*, 9690–9703. [CrossRef] [PubMed]
62. González-Carrero, S.; Guardia, M.D.L.; Galian, R.E.; Pérez-Prieto, J. Pyrene-Capped CdSe@ZnS Nanoparticles as Sensitive Flexible Oxygen Sensors in Non-Aqueous Media. *ChemistryOpen* **2014**, *3*, 199–205. [CrossRef] [PubMed]
63. Chu, C.S.; Lo, Y.L. Ratiometric fiber-optic oxygen sensors based on sol–gel matrix doped with metalloporphyrin and 7-amino-4-trifluoromethyl coumarin. *Sens. Actuators B* **2008**, *134*, 711–717. [CrossRef]
64. Cao, Y.; Koo, Y.E.L.; Kopelman, R. Poly(decyl methacrylate)-based fluorescent PEBBLE swarm nanosensors for measuring dissolved oxygen in biosamples. *Analyst* **2004**, *129*, 745–750. [CrossRef] [PubMed]
65. Koo, Y.E.L.; Cao, Y.; Kopelman, R.; Koo, S.M.; Brasuel, M.; Philbert, M.A. Real-Time Measurements of Dissolved Oxygen Inside Live Cells by Organically Modified Silicate Fluorescent Nanosensors. *Anal. Chem.* **2004**, *76*, 2498–2505. [CrossRef]
66. Wang, X.D.; Chen, X.; Xie, Z.X.; Wang, X.R. Reversible Optical Sensor Strip for Oxygen. *Angew. Chem. Int. Ed.* **2008**, *47*, 7450–7453. [CrossRef]
67. Kostov, Y.; Harms, P.; Pilato, R.S.; Rao, G. Ratiometric oxygen sensing: Detection of dual-emission ratio through a single emission filter. *Analyst* **2000**, *125*, 1175–1178. [CrossRef] [PubMed]
68. Kostov, Y.; Van Houten, K.A.; Harms, P.; Pilato, R.S.; Rao, G. Unique Oxygen Analyzer Combining a Dual Emission Probe and a Low-Cost Solid-State Ratiometric Fluorometer. *Appl. Spectrosc.* **2000**, *54*, 864–868. [CrossRef]